Insights into the complex formation of a trimeric autotransporter adhesin with a peptidoglycan-binding periplasmic protein

Shogo Yoshimoto[1], Atsuo Suzuki[1], Junichi Kanie[1], Kotaro Koiwai[1], Andrei N. Lupas[2], Katsutoshi Hori[1,*]

[1] Department of Biomolecular Engineering, Graduate School of Engineering, Nagoya University, Nagoya 464-8603, Aichi, Japan

[2] Department of Protein Evolution, Max Planck Institute for Biology, 72076 Tübingen, Baden-Württemberg, Germany

* Correspondence: Katsutoshi Hori
Department of Biomolecular Engineering, Graduate School of Engineering, Nagoya University, Furo-cho, Chikusa-ku, Nagoya, Aichi 464-8603, Japan.
Tel: +81-52-789-3339
Email: khori@chembio.nagoya-u.ac.jp

Author Contributions: K.H. and S.Y. designed the study and wrote the paper. S.Y., A.S., and K.K. prepared the recombinant proteins and conducted the structural analysis. S.Y. and A.L. conducted the bioinformatic analysis. S.Y. and J.K. conducted the other biochemical experiments. All the authors reviewed the manuscript.

Competing Interest Statement: The authors declare no competing interests.

Keywords: outer membrane protein, type V secretion system, bacterial adhesion, *Acinetobacter*

This PDF file includes:

Main Text
Figures 1 to 6

Abstract

Trimeric autotransporter adhesin (TAA) is an outer membrane (OM) protein that is widely distributed in gram-negative bacteria and is involved primarily in adhesion to biotic and abiotic surfaces, cell agglutination, and biofilm formation. TAAs are secreted onto the OM by the type Vc secretion system (SS). Because the interactions between TAAs and chaperones or special assistant proteins during secretion are short-lived, it is thought that TAAs reside on the OM without forming complexes with other proteins after secretion. In this study, we aimed to clarify the interactions between an *Acinetobacter* TAA, AtaA, and a peptidoglycan (PG)-binding periplasmic protein, TpgA, and to identify additional roles of TpgA based on these interactions. Pull-down assays using recombinant proteins identified the interacting domains. X-ray crystallography revealed the A3B3 heterohexameric complex structure of the N-terminal domain of TpgA with the transmembrane domain of AtaA and showed that both electrostatic and hydrophobic interactions contribute to stable complex formation. Bioinformatic analysis suggested that the TAA-TpgA complex is formed in a wide range of species that harbor the *taa-tpgA* gene cassette in their genome. Furthermore, the absence of TpgA increased the release of AtaA from the cell surface, suggesting that TpgA prevents the release of TAA from the cell surface via its anchoring to the PG. We propose that the TAAs that form a complex with TpgA be assigned to type Vc_2 SS, a new subtype of type Vc SS.

Significance

Gram-negative bacteria have specialized secretion systems (SSs) that translocate molecules from the cytoplasm to the extracellular space. This is the first report directly demonstrating that the transmembrane domain of a trimeric autotransporter adhesin (TAA), which is secreted by the type Vc SS, forms a stable complex with a peptidoglycan-binding periplasmic protein. This complex prevents the release of TAA from the cell surface. These results suggest that the secretion and architecture of some TAAs are more complex than was previously understood. Our work provides structural and functional insights into bacterial SSs that are important not only in microbiology but also for medical and bioengineering applications.

Main Text

Introduction

Gram-negative bacteria are enveloped by the inner membrane, peptidoglycan (PG), and outer membrane (OM) (1). To translocate molecules from the cytoplasm to the extracellular space across these barriers, gram-negative bacteria have specialized secretion systems (SSs) known as type I to VI and VIII to XI. Molecules secreted through these SSs are responsible for various functions, including cell adhesion, immune evasion, toxin activity, stress response, motility, the transfer of genetic information, and substrate degradation (2-5). Therefore, understanding the structure and function of these SSs is important not only in microbiology but also for medical and bioengineering applications.

Type V SSs have simpler architectures than that of the other types of SSs. These proteins can be further divided into subclasses, type Va to Ve SSs, which share a structure consisting of a passenger domain secreted into the extracellular space and a transmembrane domain involved in the passage of the passenger domain through the OM. (6). In the type Va SS, which secretes monomeric autotransporters, the polypeptides synthesized in the cytoplasm pass through the inner membrane via the Sec system, and periplasmic chaperones, such as SurA, Skp, and DegP, assist this periplasmic transit (7, 8). With the assistance of the β-barrel assembly machinery (BAM) complex, the transmembrane domain inserts into the OM as a 12-stranded β-barrel, and the passenger domain is transported to the extracellular milieu through the pore of the β-barrel or through a hybrid pore composed of the BAM complex and the transmembrane domain with no need for external energy sources such as ATP or a proton gradient (9). The overall secretion process of the type Vc SS, another subtype of type V SSs that secretes trimeric autotransporter adhesins (TAAs) (10), is thought to be similar to that of the type Va SS, except that a trimeric intermediate is formed before membrane insertion (11). In addition to the general periplasmic chaperones and BAM complex, in the type Vc SS, genes that form an operon with *taa* in the genome have also been reported to participate in the biogenesis of TAAs: the *Burkholderia* heptosyltransferase BimC participates in the localization of BimA to the cell pole (12), and the *Salmonella* inner membrane lipoprotein SadB participates in the outer membrane insertion of SadA (13, 14). Because the interaction between TAAs and chaperones or special assistant proteins is short-lived, TAAs are thought to reside on the outer membrane without forming stable complexes with other proteins after secretion.

91 The gram-negative bacterium *Acinetobacter* sp. Tol 5 shows extremely high
92 adhesiveness to various material surfaces, including hydrophobic plastics, hydrophilic
93 glass, and metals, through its TAA, AtaA (15). The polypeptide chains of AtaA, consisting
94 of 3,630 amino acids, form a very large homotrimeric fibrous structure that is more than 1
95 MDa in molecular weight and 260 nm in length (16). We previously reported that *tpgA*,
96 which forms a single operon with *ataA*, is involved in the secretion of AtaA (17). TpgA is a
97 periplasmic protein composed of the SmpA/OmlA-like N-terminal domain and the
98 OmpA_C-like C-terminal domain containing a PG-binding motif. Easy detection of the
99 interaction between TpgA and AtaA by a pulldown assay without crosslinking suggests that
100 TpgA binds to AtaA for a longer period than other proteins that assist in the secretion of
101 TAAs.
102 In this study, we aimed to clarify the interaction between TpgA and AtaA and to identify
103 additional roles of TpgA. This study provides structural and functional insights into PG-
104 binding periplasmic proteins that form stable complexes with TAAs. Because the *taa-tpgA*
105 gene cassette is found in a wide range of Pseudomonadota species, we propose that the
106 TAAs that form a complex with TpgA be named type Vc_2 SS.
107
108 **Results**
109 **Identification of the interacting domains of AtaA and TpgA.**
110 To identify which region of AtaA binds to TpgA, we performed a pull-down assay using
111 recombinant AtaA fragments containing several AtaA domains, as shown in Fig. 1A.
112 $AtaA_{723\text{-}806}$, $AtaA_{1221\text{-}1416}$, $AtaA_{2215\text{-}2395}$, and $AtaA_{2777\text{-}2903}$ were designed to connect to both
113 the N- and the C-terminal trimeric GCN4 adaptors, GCN4pII, which have been used to
114 stabilize coiled-coil domains of TAA recombinant proteins (18). $AtaA_{3524\text{-}3630}$ was designed
115 to be fused to the N-terminal OmpA signal sequence for secretion and presentation on the
116 outer membrane in *Escherichia coli* because it contains the transmembrane domain. We
117 also used previously constructed expression plasmids for $AtaA_{59\text{-}325}$, $AtaA_{2905\text{-}3168}$, and
118 $AtaA_{3170\text{-}3561}$ (19, 20). All of these recombinant proteins were connected to a His-tag.
119 Considering the repetitive sequences, these recombinant proteins cover almost the entire
120 region of AtaA. The cell lysate of Tol 5 Δ*ataA*, which contained native TpgA, was mixed
121 with recombinant AtaA fragment-bound nickel-nitrilotriacetic acid (Ni-NTA) beads, and the
122 pulled-down proteins were subjected to SDS–PAGE and detected by CBB staining and
123 western blotting using an anti-TpgA antibody. All of the recombinant proteins of AtaA

124 fragments immobilized on the beads were detected by CBB staining, but TpgA was
125 detected only in the sample incubated with the beads to which $AtaA_{3524-3630}$ had been bound
126 (Fig. 1B). These results suggest that TpgA specifically binds to $AtaA_{3524-3630}$, the C-terminal
127 region containing the transmembrane domain.
128 Next, to determine which domain of TpgA binds to AtaA, we performed a pull-down
129 assay using recombinant TpgA or its domains. $TpgA_{24-264}$ have been previously designed
130 with its signal sequence removed. $TpgA_{24-138}$ and $TpgA_{139-264}$ consist of the N- and C-
131 terminal domains of TpgA, respectively. All of these recombinant proteins were connected
132 to a His-tag. The cell lysate of Tol 5 Δ*tpgA*, which contained native AtaA, was mixed with
133 recombinant TpgA (or TpgA domain)-bound Ni-NTA beads, and the pulled-down proteins
134 were subjected to SDS–PAGE and detected by CBB staining and western blotting using an
135 anti-AtaA antiserum. AtaA was pulled down with $TpgA_{24-264}$ and $TpgA_{24-138}$ but not with
136 $TpgA_{139-264}$ (Fig. 1C). These results suggest that the transmembrane domain of AtaA (AtaA-
137 TM) forms a complex with the N-terminal domain of TpgA (TpgA-N).
138
139 **Crystal structure of the transmembrane domain of AtaA in complex with the N-**
140 **terminal domain of TpgA.**
141 To determine the structure of AtaA-TM in complex with TpgA-N, we attempted to purify
142 the protein complex of AtaA-TM and TpgA-N. The cell lysate of *E. coli* expressing His-
143 tagged $TpgA_{24-138}$ was added to a Ni-NTA column, which was washed to remove the
144 unbound proteins. The OmpA signal sequence-fused $AtaA_{3524-3630}$ without a His-tag was
145 expressed in *E. coli,* and the membrane fraction solubilized by a detergent was added to the
146 $TpgA_{24-138}$-bound Ni-NTA column for the formation of the protein complex. After the
147 unbound proteins were washed out, the protein complex was eluted with imidazole solution
148 and further purified by size-exclusion chromatography. As shown in Fig. 2A and 2B, highly
149 pure AtaA-TM in complex with TpgA-N was obtained at the elution peak corresponding to
150 82 kDa. This molecular weight was very close to that of 3 molecules of 11.1 kDa AtaA-TM
151 and 3 molecules of 14.9 kDa TpgA-N (78 kDa), suggesting that AtaA-TM and TpgA-N
152 form a stable A3B3 heterohexamer complex.
153 After crystallization screens using the purified protein complex, we determined the
154 structure of AtaA-TM in complex with TpgA-N at 2.6 Å resolution by X-ray
155 crystallography (Fig. 2C, PDB ID: 8WX9). This is the first report showing a quaternary
156 structure of the transmembrane domain of TAA in complex with another protein. Three

157 molecules of TpgA-N bind to the periplasmic side of the homotrimeric transmembrane β-
158 barrel of AtaA-TM, forming the A3B3 heterohexamer, as estimated by size exclusion
159 chromatography. The monomer of AtaA-TM contains an N-terminal helix followed by a
160 four-stranded β-sheet, and a 12-stranded β-barrel is formed through homotrimerization. As
161 shown in Figure 2D, the structure of AtaA-TM is very similar to the previously determined
162 structures of folded transmembrane domains of other TAAs, such as those of *Haemophilus*
163 *influenzae* Hia and *Yersinia enterocolitica* YadA (21, 22). The structure of TpgA-N consists
164 of two small α-helices and three antiparallel β-strands with an ααβββ topology (Fig. 2E).
165 The two α-helices pack against the β-sheet, forming an α/β 2-layer sandwich architecture.
166 The most similar known structure is that of *E. coli* BamE (23), which shares 27% sequence
167 identity (Fig. 2F). However, the structures differ, particularly in the N-terminal region and
168 in the β1- and β2-strands, which are involved in the binding of BamE to BamA and BamD
169 (24).
170
171 **Interaction between the transmembrane domain of AtaA and the N-terminal domain**
172 **of TpgA.**
173 Several interactions between AtaA-TM and TpgA-N were observed in the crystal
174 structure (Fig. 3A). The charged side chains of K64 and D65 in the α2-helix of TpgA
175 electrostatically interact with the side chains of D3601 in the β2-β3 loop and K3576 in the
176 β1-strand of AtaA, respectively. The α2-β1 loop of TpgA extends to the transmembrane
177 region of the β-barrel of AtaA-TM, and the hydrophobic tip composed of L80 and F81 of
178 TpgA interacts with hydrophobic residues on the outside of the AtaA β-barrel. To examine
179 the extent to which these interactions contribute to complex formation, we performed a
180 pull-down assay using point-mutated TpgA-N proteins. The cell lysate of Tol 5 Δ*tpgA*,
181 which contained native AtaA, was mixed with mutated TpgA-bound Ni-NTA beads, and the
182 pulled-down proteins were subjected to SDS–PAGE and detected by CBB staining. As
183 shown in Fig. 3B, the D65A and L80A mutations did not affect complex formation between
184 AtaA-TM and TpgA-N, but the K64A and F81A mutations reduced complex formation.
185 The K64A/D65A and L80A/F81A double mutations markedly reduced the interaction.
186 These results indicate that both electrostatic and hydrophobic interactions caused by these
187 residues, especially K64 and F81 of TpgA, are important for complex formation.
188
189 **Bioinformatic analysis of the AtaA-TpgA interaction.**

190 To clarify whether the TAA-TpgA complex exists in a wide range of species, we
191 performed bioinformatic analysis. The amino acid sequences with similarity to that of
192 TpgA-N were collected using BLAST and clustered based on sequence similarity using
193 CLANS (25). As shown in Fig. 4A, eight clusters were observed. TpgA-like sequences
194 formed cluster I, which was different from clusters II and III containing a typical
195 SmpA/OmlA family protein, BamE. Cluster I included sequences from a wide range of
196 Pseudomonadota (Proteobacteria), such as *Altererythrobacter*, *Burkholderia*, *Neisseria*,
197 *Acinetobacter*, *Stenotrophomonas*, *Escherichia*, and *Campylobacter*, as shown in Table S1.
198 The domain composition of the sequences differed from cluster to cluster (Fig. 4A). In
199 cluster I, approximately 80% of the sequences have an OmpA_C domain in the C-terminus,
200 similar to that in TpgA, and most of the sequences in clusters II, III, IV, and V have no
201 extra domain. Those in clusters VI and VII have a domain of unknown function (DUF) in
202 the N-terminus, and those in cluster VIII have a DUF in the C-terminus. Thus, the domain
203 structure of the sequences in cluster I, including TpgA, which consists of an N-terminal
204 SmpA/OmlA domain and a C-terminal OmpA_C domain, is distinct and unique among
205 proteins that contain the SmpA/OmlA domain.
206 In addition, 91% of the sequences in cluster I were downstream of the *taa* gene in the
207 genome, although those in other clusters were rarely near the *taa* gene. This result is
208 consistent with a previous finding that the occurrence of *ata*, a TAA of *Acinetobacter*
209 *baumannii*, in the genome was tightly linked to that of *tpgA* (26). In the *taa-tpgA* gene
210 cassette found in cluster I, L80 and F81 of TpgA were conserved as hydrophobic and
211 aromatic residue pairs, respectively (Fig. 4B). Furthermore, K64 of TpgA and D3601 of
212 AtaA, which interact with each other, are also conserved (Fig. 4B, C). In contrast, D3601 is
213 not conserved in TAAs that do not form the *taa-tpgA* gene cassette, such as YadA, BadA, or
214 UpaG, except for Hia, suggesting that D3601 of TAAs for which *tpgA* exists downstream in
215 the genome, is conserved because of its interaction with TpgA. These results suggest that
216 the TAA-TpgA protein complex is formed in a wide range of species that have a *taa-tpgA*
217 gene cassette in their genome.
218
219 **AtaA is more easily released from the cell surface in the *tpgA*-deficient strain.**
220 Because TpgA not only binds to PG (17) but also forms a stable complex with AtaA-TM,
221 AtaA may be tightly anchored to the outer membrane by TpgA. We therefore investigated
222 whether the deletion of *tpgA* would facilitate the release of AtaA from the cell surface under

223 shear stress, which causes a large mechanical load on AtaA due to its adhesiveness. When
224 the cell suspensions were mixed by inversion using a rotary mixer in BS-N buffer and
225 subjected to SDS–PAGE, only a small amount of AtaA was detected in the supernatant of
226 the Tol 5 WT cell suspension, but a large amount of AtaA was detected in the supernatant of
227 the *tpgA*-deficient strain cell suspension (Fig. 5). In contrast, after mixing by inversion in
228 BS-N buffer supplemented with 1% casamino acids, an adhesion inhibitor of AtaA (27) that
229 reduces the mechanical load on AtaA, no AtaA was detected in the supernatant of either
230 strain. These results indicate that TpgA plays a role in anchoring AtaA tightly to the cell
231 surface and preventing the release of AtaA under shear stress.
232
233 **Discussion**
234 TAAs interact with various assistant proteins during secretion but are thought to consist of
235 simple components after secretion. In this study, we revealed that the N-terminal domain of
236 TpgA forms a heterohexamer with the folded AtaA-TM (Fig. 2). This is the first report
237 directly showing that the transmembrane domain of TAA forms a stable complex with
238 periplasmic proteins. During the secretion of TAAs, the partially folded trimer in the
239 periplasmic space is likely inserted into the outer membrane, after which the PSD passes
240 through the open-state pore, and the β-barrel closes to complete secretion (11). Considering
241 that TpgA promotes secretion after insertion into the outer membrane (17), TpgA binds to
242 the partially folded trimer of AtaA-TM, forming an open-state pore and promoting the
243 passage of PSD through the pore. After the secretion of the PSD, TpgA continues to bind to
244 the closed AtaA-TM pore and prevent the release of AtaA. Therefore, the secretion process
245 of TAAs, at least in part, may be more complex than previously expected.
246 While each SS of type Va to Ve secretes a variety of passenger domains into the
247 extracellular space, they share a common feature in that the transmembrane domain is
248 anchored only to the OM, except for some type Ve SSs, which have a PG-binding LysM
249 domain on the periplasmic side (28). TpgA also contains another type of PG-binding
250 domain, the OmpA_C-like domain, at the C-terminus, which actually binds to PG (17).
251 Considering that the N-terminal domain of TpgA binds to the C-terminal transmembrane
252 domain of AtaA (Figs. 1, 2), these proteins likely form the AtaA-TpgA-PG complex. In
253 mammalian cells, the cell adhesion protein cadherin also forms a complex with an actin
254 filament via catenins (29, 30). This implies that anchoring cell adhesion proteins to the
255 structures involved in cell shape and strength, such as the cytoskeleton or peptidoglycan,

256 would be universally important for stabilizing these proteins under mechanical load.
257 The overall structure of TpgA-N was similar to that of BamE, but the structures of the
258 regions of BamE that bind to BamA and BamD and the corresponding region of TpgA-N
259 were different (Fig. 2F). Furthermore, clustering analysis revealed that the *tpgA*-like genes
260 formed a distinct cluster from other SmpA/OmlA family genes, such as *bamE* (Fig. 4A).
261 These results indicate that the function of TpgA is completely different from that of BamE
262 as a subunit of the BAM complex. In fact, TpgA was found to participate in anchoring AtaA
263 to the OM as well as in secretion (Fig. 5). In addition, *tpgA*-like genes were found in a wide
264 range of Pseudomonadota (Proteobacteria), and most of them were located downstream of
265 the *taa* genes in the genome (Fig. 4 and Table S1). Therefore, considering the uniqueness
266 and generality of TpgA, we propose that TAAs that form a complex with TpgA be named
267 type Vc_2 SS, a new subtype of type Vc (Fig. 6).
268 In conclusion, we revealed the structure of a PG-binding periplasmic protein that forms a
269 stable complex with the transmembrane domain of a TAA and demonstrated that this
270 protein participates in anchoring the TAA to the cell surface. Our findings will contribute to
271 a better understanding of the type Vc SS and the control of TAA-mediated adhesion, which
272 is important for medical and engineering applications.
273
274
275 **Materials and Methods**
276 **Bacterial strains and growth conditions.**
277 The bacterial strains and plasmids used in this study are listed in Table S2. *Acinetobacter*
278 sp. Tol 5 and its derivative strains were grown in basal salt medium supplemented with
279 toluene or in Luria–Bertani (LB) medium at 28°C, as described previously (15). *E. coli*
280 DH5α, BL21(DE3), and their derivative strains were grown in LB medium supplemented
281 with 100 μg/ml ampicillin for cells harboring pASK-IBA plasmids or with 50 μg/ml
282 kanamycin for cells harboring pET plasmids at 37°C.
283
284 **Construction of plasmids.**
285 The primers used in this study are listed in Table S3. To construct plasmids expressing a
286 recombinant AtaA fragment fused to a GCN4pII-tag at both the N- and C-termini and a
287 His-tag at the C-terminus, DNA fragments encoding $AtaA_{723\text{-}806}$, $AtaA_{1221\text{-}1416}$, $AtaA_{2215\text{-}2395}$,
288 or $AtaA_{2777\text{-}2903}$ were amplified via PCR and inserted into the BsaI site of the *E. coli*

289 expression vector pIBA-GCN4tri-His (18). To construct a plasmid expressing $AtaA_{3524-3630}$
290 fused to the His-tag at the N-terminus at the OM, the DNA fragment encoding this gene
291 was amplified via PCR and inserted between the NheI and HindIII sites of the *E. coli*
292 expression vector pASK-IBA12 (IBA Lifesciences, Göttingen, Germany), generating
293 pIBA-$AtaA_{3524-3630}$-His. To remove the His-tag sequence from pIBA-$AtaA_{3524-3630}$-His, a
294 DNA fragment was amplified via PCR using pIBA-$AtaA_{3524-3630}$-His as a template with two
295 primers (TM-dHis-f/r) and then self-ligated, generating pIBA-$AtaA_{3524-3630}$. To construct
296 plasmids expressing $TpgA_{24-138}$ or $TpgA_{139-264}$ fused to a His-tag, a DNA fragment was
297 amplified via PCR using pET28d::$TpgA_{24-264}$ (19) as a template with two primer sets
298 (TpgA-N-f/r or TpgA-C-f/r) and then self-ligated, generating pET28d::$TpgA_{24-138}$ and
299 pET28d::$TpgA_{139-264}$.
300
301 **Protein purification.**
302 To purify the complex of TpgA-N and AtaA-TM, an overnight culture of BL21 (DE3;
303 pET28d::$TpgA_{24-264}$) was diluted 1:100 in LB medium and incubated for 3 h at 37°C. After
304 incubation, isopropyl β-D-thiogalactopyranoside (IPTG) (final concentration: 0.1 mM) was
305 added to the medium, and the culture was further incubated at 18°C for 18 h. The cells were
306 harvested by centrifugation at 5,000×*g* at 4°C for 15 min, resuspended in lysis buffer (25
307 mM Tris-HCl, 150 mM NaCl, 20 mM imidazole, pH 9.0) supplemented with 0.1 mg/ml
308 lysozyme, and lysed using a high-pressure homogenizer (LAB 2000; SMT Co., Tokyo,
309 Japan) at 1,000 bar for 10 min. After centrifugation at 10,000×*g* at 4°C for 15 min, the
310 supernatant was loaded onto a Ni-NTA Superflow column (Qiagen, Venlo, Netherlands),
311 and the unbound proteins were washed off with lysis buffer. Subsequently, an overnight
312 culture of BL21 (DE3; pIBA-$AtaA_{3524-3630}$) was diluted 1:100 in LB medium and incubated
313 for 3 h at 37°C. After incubation, anhydrotetracycline (AHTC) (final concentration: 0.2
314 μg/ml) was added to the medium, and the mixture was further incubated at 28°C for 12 h.
315 The cells were harvested by centrifugation at 5,000×*g* at 4°C for 15 min, resuspended in
316 lysis buffer supplemented with 0.1 mg/ml lysozyme, and lysed using a high-pressure
317 homogenizer at 1,000 bar for 10 min. After centrifugation at 5,000×*g* at 4°C for 15 min, the
318 supernatant was ultracentrifuged at 100,000×*g* at 4°C for 2 h, and the precipitate was
319 solubilized with 5% Elugent (Merck, Darmstadt, Germany) and suspended in Elugent
320 buffer A (25 mM Tris-HCl, 150 mM NaCl, 20 mM imidazole, 0.5% Elugent, pH 9.0). The
321 suspension was loaded onto a TpgA-N-bound Ni-NTA column, and unbound proteins were

322 washed off with Elugent buffer A. The bound proteins were eluted with Elugent buffer A
323 supplemented with 300 mM imidazole and loaded onto a HiLoad 26/60 Superdex 75 pg
324 column (Cytiva, Marlborough, MA) equilibrated with 25 mM Tris-HCl (pH 7.5) buffer
325 containing 10 mM NaCl and 0.5% Elugent. Peak fractions containing the protein complex
326 were dialyzed using a 12-14 kD MWCO dialysis membrane (Spectrum Laboratories,
327 Rancho Dominguez, CA) against Elugent buffer B (25 mM Tris-HCl, 10 mM NaCl, 0.5%
328 Elugent, pH 9.0) and loaded onto a HiTrap Q HP column (Cytiva) equilibrated with Elugent
329 buffer B. The column was washed three times with 0.6% tetraethylene glycol monooctyl
330 ether (C8E4) containing 25 mM Tris-HCl (pH 9.0) and 10 mM NaCl and two times with
331 0.6% C8E4 containing 25 mM Tris-HCl (pH 9.0) and 100 mM NaCl. The bound proteins
332 were eluted with 0.6% C8E4 containing 25 mM Tris-HCl (pH 9.0) and 500 mM NaCl,
333 dialyzed against crystallization buffer (25 mM Tris-HCl, 10 mM NaCl, 0.6% C8E4, pH
334 8.0), and concentrated by ultrafiltration using a 10 kDa cutoff filter device (Amicon Ultra;
335 Merck).
336 $TpgA_{24-264}$, $TpgA_{24-138}$ (TpgA-N), and $TpgA_{139-264}$ (TpgA-C) were purified as described
337 previously (17). In brief, cells expressing each protein were harvested and lysed using a
338 high-pressure homogenizer. After centrifugation, the protein was purified from the
339 supernatant by Ni-affinity chromatography, ion-exchange chromatography, and size-
340 exclusion chromatography.
341
342 **Pull-down assay.**
343 For the pull-down assay using recombinant AtaA fragments and cell lysate containing
344 TpgA, an overnight culture of BL21 (DE3) cells harboring plasmids expressing
345 recombinant AtaA fragments was diluted 1:100 in LB medium and incubated for 3 h at
346 37°C. After incubation, AHTC (final concentration: 0.2 μg/ml) was added to the medium
347 and further incubated at 28°C for 12 h. The cells were harvested by centrifugation at
348 5,000×*g* at 4°C for 15 min, resuspended in pull-down buffer A (25 mM Tris-HCl, 10 mM
349 NaCl, 0.1% Tween 20, 20 mM imidazole, pH 7.5), and lysed by sonication. After
350 centrifugation at 10,000×*g* at 4°C for 10 min, 500 μl of the supernatant (2 mg/ml) was
351 mixed with 10 μl of Ni-NTA Superflow. After 2 h of incubation on a rotary mixer (NRC-
352 20D; Nissinrika, Tokyo, Japan) at 5 rpm and 4°C, the beads were pelleted by centrifugation
353 at 1,000×*g* for 1 min at 4°C and rinsed three times with pull-down buffer A. The beads were
354 mixed with 500 μl of 5 mg/ml cell lysate from Tol 5 Δ*ataA* and incubated for 2 h on a

355 rotary mixer at 4°C. The beads were pelleted by centrifugation at 1,000×*g* for 1 min at 4°C
356 and rinsed three times with pull-down buffer A. The bound proteins were eluted with 50 μl
357 of 300 mM imidazole (pH 7.5), mixed with 50 μl of 2×SDS–PAGE sample buffer, and
358 boiled at 98°C for 10 min. The protein samples were separated by SDS–PAGE and
359 subjected to CBB staining and western blotting analysis with an anti-TpgA antibody (17).
360 For the pull-down assay using recombinant TpgA fragments and cell lysate containing
361 AtaA, 50 μg of His-tagged $TpgA_{24-264}$, His-tagged $TpgA_{24-138}$, or His-tagged $TpgA_{139-264}$
362 suspended in 300 μl of pull-down buffer A was mixed with 10 μl of Ni-NTA Superflow.
363 After 1 h of incubation on a rotary mixer at 4°C, the beads were pelleted by centrifugation
364 at 1,000×*g* for 1 min at 4°C, rinsed three times with pull-down buffer A, and resuspended in
365 300 μl of pull-down buffer A. To prepare the cell lysate of Tol 5 Δ*tpgA*, 100 ml of the cell
366 suspension at an OD_{660} of 0.6 was harvested by centrifugation at 5,000×*g* for 10 min at 4°C
367 and resuspended in 2 ml of BugBuster (Merck), and 50 μg/ml lysozyme and 1 mM
368 phenylmethanesulfonyl fluoride (PMSF) were added. Unlysed cells and debris were
369 removed by centrifugation at 10,000×*g* for 10 min at 4°C. Finally, 200 μl of the cell lysate
370 was mixed with 300 μl of TpgA fragment-bound Ni-NTA beads suspended in pull-down
371 buffer A and incubated on a rotary mixer at 4°C for 2 h. The beads were pelleted by
372 centrifugation at 1,000×*g* for 1 min at 4°C and rinsed with pull-down buffer A for removal
373 of unbound proteins. The bound proteins were eluted with 50 μl of 300 mM imidazole (pH
374 7.5), mixed with 50 μl of 2×SDS–PAGE sample buffer, and boiled at 98°C for 10 min. The
375 protein samples were separated via SDS–PAGE and subjected to CBB staining and western
376 blotting analysis with anti- $AtaA_{699-1014}$ antiserum.
377 For the pull-down assay using TpgA mutants and cell lysates containing AtaA-TM, 10 μg
378 of His-tagged TpgA variants suspended in 1 ml of pull-down buffer B (25 mM Tris-HCl,
379 150 mM NaCl, 20 mM imidazole, 0.6% Elugent, pH 7.0) was mixed with 10 μl of Ni-NTA
380 Superflow. After a 1-h incubation on a rotary mixer at 4°C, the beads were pelleted by
381 centrifugation at 1,000×*g* for 1 min at 4°C and rinsed three times with pull-down buffer B.
382 The beads were mixed with 1 ml of 1 mg/ml cell lysate containing AtaA-TM suspended in
383 pull-down buffer B and incubated for 1 h on a rotary mixer at 4°C. The beads were pelleted
384 by centrifugation at 1,000×*g* for 1 min at 4°C and rinsed three times with pull-down buffer
385 B. The bound proteins were then eluted with 25 μl of 500 mM imidazole (pH 7.5), mixed
386 with 25 μl of 2×SDS–PAGE sample buffer, and boiled at 98°C for 10 min. The protein
387 samples were separated by SDS–PAGE and subjected to CBB staining.

388

389 **Crystallization and X-ray crystallography.**

390 The crystallization conditions for the purified protein were first screened by using the
391 sitting-drop vapor-diffusion method at 20°C under 240 conditions using MemPlus
392 (Molecular Dimensions, Sheffield, UK), MemGold (Molecular Dimensions), and The
393 Protein Complex Suite (Qiagen). One microliter of 4.6 mg/ml protein sample suspended in
394 crystallization buffer (25 mM Tris-HCl, 10 mM NaCl, 0.6% C8E4, pH 8.0) and 1 μl of
395 reservoir solution were mixed and periodically observed for 2 weeks under a polarized
396 microscope (BH-2; Olympus). The final optimized crystallization conditions were as
397 follows: 0.2 M MES, 0.4 M calcium chloride, and 35% polyethylene glycol 400 at pH 5.0.
398 The crystal was loop-mounted and quenched in liquid nitrogen. The diffraction of the
399 crystals was measured under a cryo-condition at the synchrotron beamline NW-12A of the
400 Photon Factory (Tsukuba, Japan) by using a CCD detector (Quantum 270; ADSC, Poway,
401 CA). Diffraction images were processed and scaled by using HKL2000. The CCP4
402 program suite was used for model building and refinement. The phases of all the structures
403 were determined by molecular replacement using MOLREP. The structure was solved using
404 the Hia transmembrane domain (PDB: 2GR7) as the search model. After the molecular
405 replacement, the structures were automatically built by ARP/wARP, manually modeled
406 with Coot, and refined by REFMAC5 and PHENIX. The crystallographic parameters are
407 summarized in Table S4. The final coordinates and structure factors that support the
408 findings of this study have been deposited in the PDB with the accession code 8WX9.

409

410 **Bioinformatics.**

411 To obtain sequences with similarity to the N-terminal domain of TpgA, the NR70 database
412 was searched for the amino acid sequence of $TpgA_{24\text{-}138}$ using PSI-BLAST on the MPI
413 Bioinformatics Toolkit (31). We retrieved 1461 sequences (E-value <0.001), and the
414 retrieved sequences were clustered using CLANS (25) at a P-value cutoff of 1e-10, an
415 attract value of 10 and a repulse value of 10. The multiple sequence alignment was
416 generated using ClustalO. The DNA sequence of *taa*, which is encoded upstream of the
417 *tpgA*-like gene, was collected from the NCBI nucleotide database. We searched for protein
418 structures similar to that of TpgA-N via the Dali server (32).

419

420 **Protein release assay.**

One milliliter of bacterial cell suspension in BS-N buffer (34.5 mM Na_2HPO_4, 14.7 mM KH_2PO_4, 15.5 mM K_2SO_4, pH 7.2) or BS-N buffer supplemented with 1% casein hydrolysate (casamino acids technical grade; Becton, Dickinson and Company, NJ, USA) at an OD_{660} of 4.0 was transferred to a ProteoSave SS 1.5-mL centrifuge tube (Sumitomo Bakelite, Tokyo, Japan). The cell suspension was then mixed by inversion using a rotary mixer (RT-50; Taitec, Saitama, Japan) at 4°C for 36 h at 30 rpm. After incubation, the suspension was centrifuged at 5,000×g and 4°C for 10 min to remove cells. The supernatant was carefully transferred to a new tube and centrifuged at 15,000×g at 4°C for 15 min to remove debris. Then, 900 µl of the clarified supernatant was transferred to a new 1.5 ml tube. Proteins in the supernatant were concentrated by trichloroacetic acid (TCA) precipitation and subsequently analyzed via SDS–PAGE.

Data Availability

Crystallographic coordinates and structure factors have been deposited in the PDB under accession code 8WX9.

Acknowledgments

We thank Jens Bassler, Ryuta Hiroshige and Ayumi Hayashi for their technical assistance. We also thank Dirk Linke of the University of Oslo and Masahito Ishikawa of Nagahama Institute of Bio-Science and Technology for helpful discussion. This work was supported by the Japan Society for the Promotion of Science (JSPS) KAKENHI (Grant Number JP21H05227).

References

1. J. W. Sun, S. T. Rutherford, T. J. Silhavy, K. C. Huang, Physical properties of the bacterial outer membrane. *Nat Rev Microbiol* **20**, 236-248 (2022).
2. T. R. D. Costa *et al.*, Secretion systems in Gram-negative bacteria: structural and mechanistic insights. *Nat Rev Microbiol* **13**, 343-359 (2015).
3. T. Palmer, A. J. Finney, C. K. Saha, G. C. Atkinson, F. Sargent, A holin/peptidoglycan hydrolase-dependent protein secretion system. *Mol Microbiol* **115**, 345-355 (2021).
4. A. S. Grossman, T. J. Mauer, K. T. Forest, H. Goodrich-Blair, A widespread bacterial secretion system with diverse substrates. *Mbio* **12**, e0195621 (2021).

455 5. A. M. Lasica, M. Ksiazek, M. Madej, J. Potempa, The type IX secretion system
456 (T9SS): Highlights and recent insights into its structure and function. *Front Cell*
457 *Infect Microbiol* **7**, 215 (2017).
458 6. J. C. Leo, I. Grin, D. Linke, Type V secretion: mechanism(s) of autotransport
459 through the bacterial outer membrane. *Philos T R Soc B* **367**, 1088-1101 (2012).
460 7. G. E. Purdy, C. R. Fisher, S. M. Payne, IcsA surface presentation in *Shigella flexneri*
461 requires the periplasmic chaperones DegP, Skp, and SurA. *J Bacteriol* **189**, 5566-
462 5573 (2007).
463 8. F. Ruiz-Perez *et al.*, Roles of periplasmic chaperone proteins in the biogenesis of
464 serine protease autotransporters of *Enterobacteriaceae*. *J Bacteriol* **191**, 6571-6583
465 (2009).
466 9. H. D. Bernstein, Type V secretion in Gram-negative bacteria. *EcoSal Plus* **8**,
467 doi:10.1128/ecosalplus.ESP-0031-2018 (2019).
468 10. D. Linke, T. Riess, I. B. Autenrieth, A. Lupas, V. A. J. Kempf, Trimeric
469 autotransporter adhesins: variable structure, common function. *Trends Microbiol* **14**,
470 264-270 (2006).
471 11. R. Sikdar, J. H. Peterson, D. E. Anderson, H. D. Bernstein, Folding of a bacterial
472 integral outer membrane protein is initiated in the periplasm. *Nat Commun* **8**, 1309
473 (2017).
474 12. Q. Lu, Y. Xu, Q. Yao, M. Niu, F. Shao, A polar-localized iron-binding protein
475 determines the polar targeting of *Burkholderia* BimA autotransporter and actin tail
476 formation. *Cell Microbiol* **17**, 408-424 (2015).
477 13. I. Grin *et al.*, A trimeric lipoprotein assists in trimeric autotransporter biogenesis in
478 *Enterobacteria*. *J Biol Chem* **289**, 7388-7398 (2014).
479 14. M. D. Hartmann *et al.*, Complete fiber structures of complex trimeric
480 autotransporter adhesins conserved in enterobacteria. *Proc Natl Acad Sci USA* **109**,
481 20907-20912 (2012).
482 15. M. Ishikawa, H. Nakatani, K. Hori, AtaA, a new member of the trimeric
483 autotransporter adhesins from *Acinetobacter* sp. Tol 5 mediating high adhesiveness
484 to various abiotic surfaces. *PLoS One* **7**, e48830 (2012).
485 16. S. Yoshimoto, H. Nakatani, K. Iwasaki, K. Hori, An *Acinetobacter* trimeric
486 autotransporter adhesin reaped from cells exhibits its nonspecific stickiness via a
487 highly stable 3D structure. *Sci Rep* **6**, 28020 (2016).

488 17. M. Ishikawa, S. Yoshimoto, A. Hayashi, J. Kanie, K. Hori, Discovery of a novel
489 periplasmic protein that forms a complex with a trimeric autotransporter adhesin
490 and peptidoglycan. *Mol Microbiol* **101**, 394-410 (2016).
491 18. B. H. Alvarez *et al.*, A new expression system for protein crystallization using
492 trimeric coiled-coil adaptors. *Protein Eng Des Sel* **21**, 11-18 (2008).
493 19. K. Koiwai, M. D. Hartmann, D. Linke, A. N. Lupas, K. Hori, Structural basis for
494 toughness and flexibility in the C-terminal passenger domain of an *Acinetobacter*
495 trimeric autotransporter adhesin. *J Biol Chem* **291**, 3705-3724 (2016).
496 20. S. Aoki *et al.*, Native display of a huge homotrimeric protein fiber on the cell
497 surface after precise domain deletion. *J Biosci Bioeng* **129**, 412-417 (2020).
498 21. G. Meng, N. K. Surana, J. W. St Geme, 3rd, G. Waksman, Structure of the outer
499 membrane translocator domain of the *Haemophilus influenzae* Hia trimeric
500 autotransporter. *EMBO J* **25**, 2297-2304 (2006).
501 22. S. A. Shahid *et al.*, Solid-state NMR study of the YadA membrane-anchor domain in
502 the bacterial outer membrane. *Angew Chem Int Ed* **54**, 12602-12606 (2015).
503 23. Y. Gu *et al.*, Structural basis of outer membrane protein insertion by the BAM
504 complex. *Nature* **531**, 64-69 (2016).
505 24. S. Kumar, A. Konovalova, BamE directly interacts with BamA and BamD
506 coordinating their functions. *Mol Microbiol* **120**, 397-407 (2023).
507 25. T. Frickey, A. Lupas, CLANS: a Java application for visualizing protein families
508 based on pairwise similarity. *Bioinformatics* **20**, 3702-3704 (2004).
509 26. M. Weidensdorfer *et al.*, The *Acinetobacter* trimeric autotransporter adhesin Ata
510 controls key virulence traits of *Acinetobacter baumannii*. *Virulence* **10**, 68-81
511 (2019).
512 27. Y. Ohara, S. Yoshimoto, K. Hori, Control of AtaA-mediated bacterial
513 immobilization by casein hydrolysates. *J Biosci Bioeng* **128**, 544-550 (2019).
514 28. J. C. Leo *et al.*, The Intimin periplasmic domain mediates dimerisation and binding
515 to peptidoglycan. *Mol Microbiol* **95**, 80-100 (2015).
516 29. S. Pokutta, W. I. Weis, Structure and mechanism of cadherins and catenins in cell-
517 cell contacts. *Annu Rev Cell Dev Biol* **23**, 237-261 (2007).
518 30. J. M. Gooding, K. L. Yap, M. Ikura, The cadherin-catenin complex as a focal point
519 of cell adhesion and signalling: new insights from three-dimensional structures.
520 *BioEssays* **26**, 497-511 (2004).

31. L. Zimmermann *et al.*, A completely reimplemented MPI Bioinformatics Toolkit with a new HHpred server at its core. *J Mol Biol* **430**, 2237-2243 (2018).
32. L. Holm, DALI and the persistence of protein shape. *Protein Sci* **29**, 128-140 (2020).

527 **Figure legends**

528

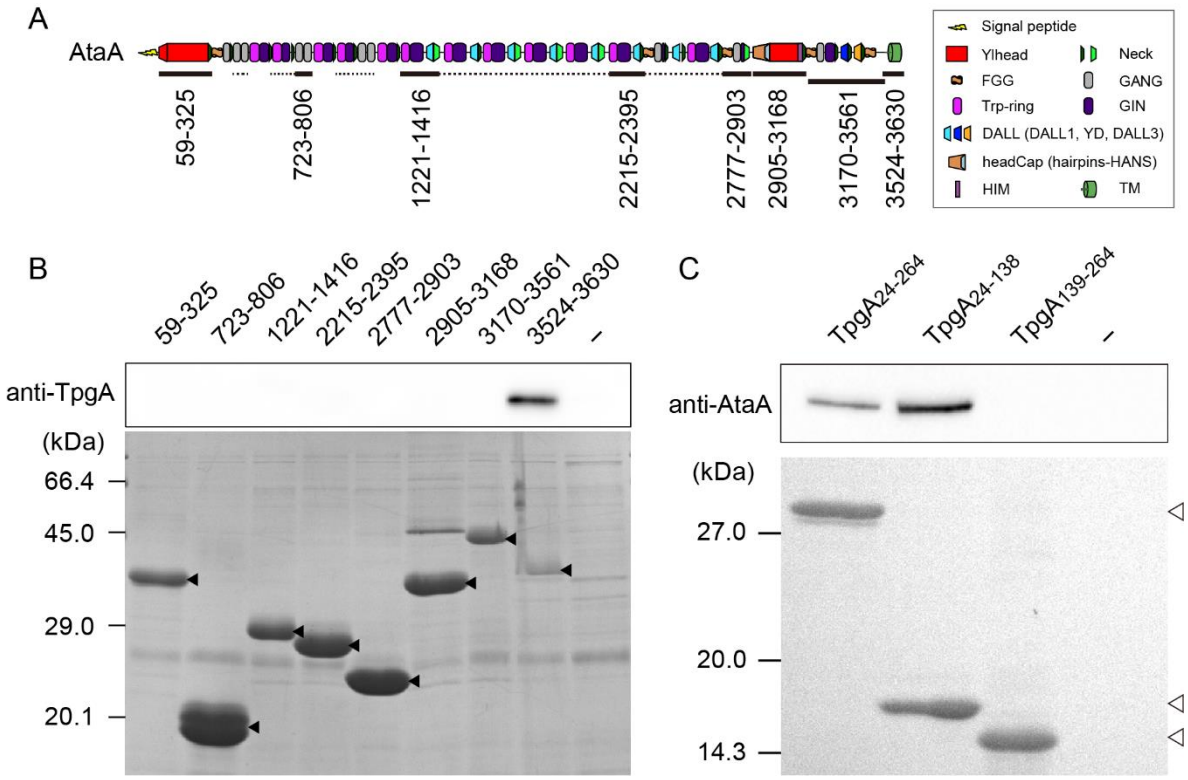

529

530 **Figure 1. Identification of the interacting domains of AtaA and TpgA.** (A) Schematic
531 structure of AtaA. The black lines show the region where the recombinant protein was
532 constructed, and the dotted lines show the region with high sequence similarity (>50%) to
533 the recombinant proteins. (B) Pull-down assay using recombinant AtaA fragments and
534 TpgA-containing cell lysate. The cell lysate of Tol 5 Δ*ataA* was mixed with recombinant
535 AtaA fragment-bound Ni-NTA beads or untreated beads (-). The pulled-down proteins were
536 subjected to SDS–PAGE and analyzed by western blotting to detect TpgA and CBB
537 staining to detect AtaA fragments. The solid triangles indicate recombinant AtaA
538 fragments. The upper numbers indicate the amino acid numbers of each recombinant AtaA
539 fragment immobilized onto Ni-NTA beads. (C) Pull-down assay using recombinant TpgA
540 fragments and AtaA-containing cell lysate. The cell lysate of Tol 5 Δ*tpgA* was mixed with
541 recombinant TpgA fragment-bound Ni-NTA beads or untreated beads (-). The pulled-down
542 proteins were subjected to SDS–PAGE and analyzed by western blotting to detect AtaA and
543 CBB staining to detect TpgA fragments. The open triangles indicate recombinant TpgA
544 fragments.

545

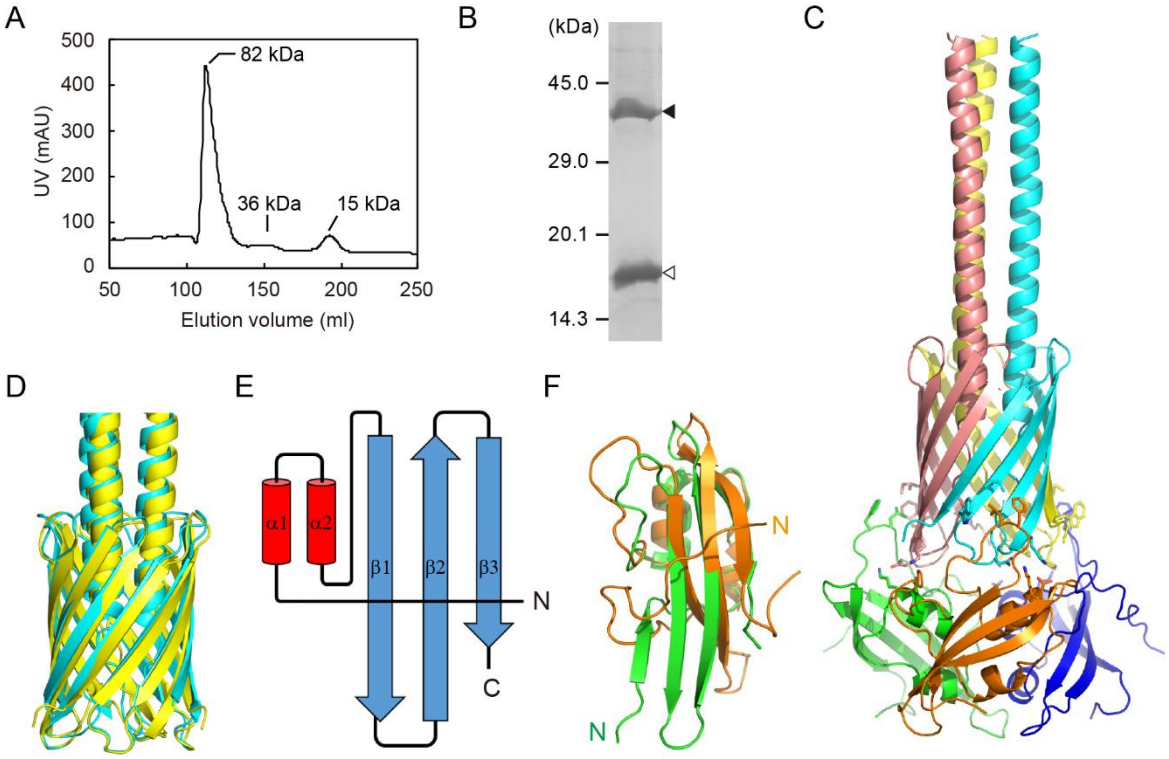

Figure 2. Crystal structure of the transmembrane domain of AtaA in complex with the N-terminal domain of TpgA. (A) Size-exclusion chromatography of the complex of AtaA-TM and TpgA-N. (B) The purified complex of AtaA-TM and TpgA-N was subjected to SDS–PAGE followed by CBB staining. The solid and open triangles indicate the AtaA-TM trimer and TpgA-N, respectively. (C) Overall structure of the AtaA-TM and TpgA-N complex. The AtaA-TM monomers are shown in cyan, pink and yellow, and the TpgA-N monomers are shown in orange, green and blue, respectively. (D) Comparison of AtaA-TM (yellow) with the transmembrane domain of *H. influenzae* Hia (2GR7; cyan). (E) A topology diagram of TpgA-N. α-helices are shown as cylinders, and β-strands are shown as arrows. (F) Comparison of TpgA-N (orange) with *E. coli* BamE (5D0Q; green).

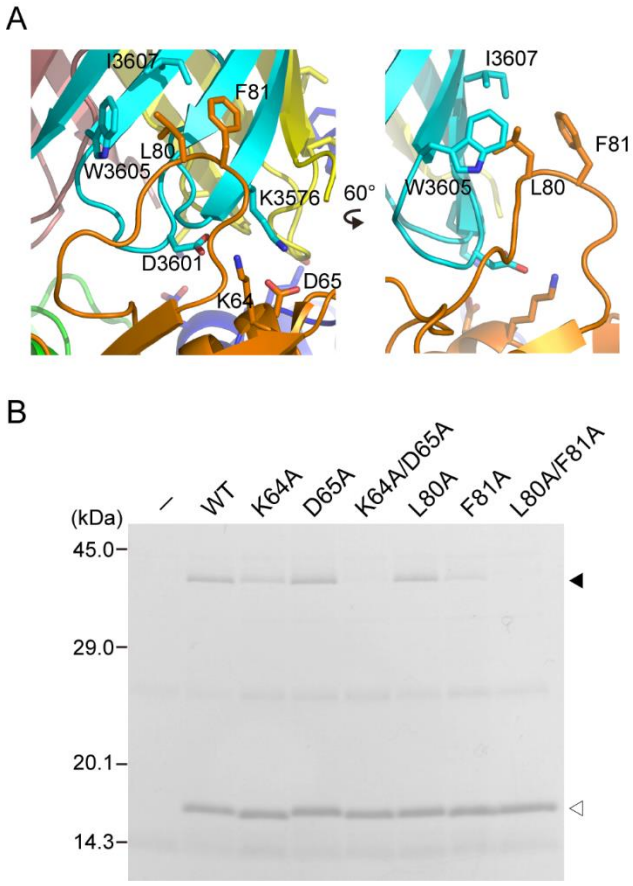

Figure 3. Interaction between the transmembrane domain of AtaA and the N-terminal domain of TpgA. (A) Enlarged views showing hydrophobic and electrostatic interactions between AtaA-TM (cyan) and TpgA-N (orange). The interacting residues are shown in stick representation. (B) Pull-down assay of AtaA-TM and mutated TpgA-N. Cell lysate containing AtaA-TM was mixed with His-tagged TpgA-N-bound Ni-NTA beads or untreated beads as a control (-). The pulled-down proteins were subjected to SDS–PAGE and detected by CBB staining. The solid and open triangles indicate the AtaA-TM and point-mutated TpgA-N proteins, respectively.

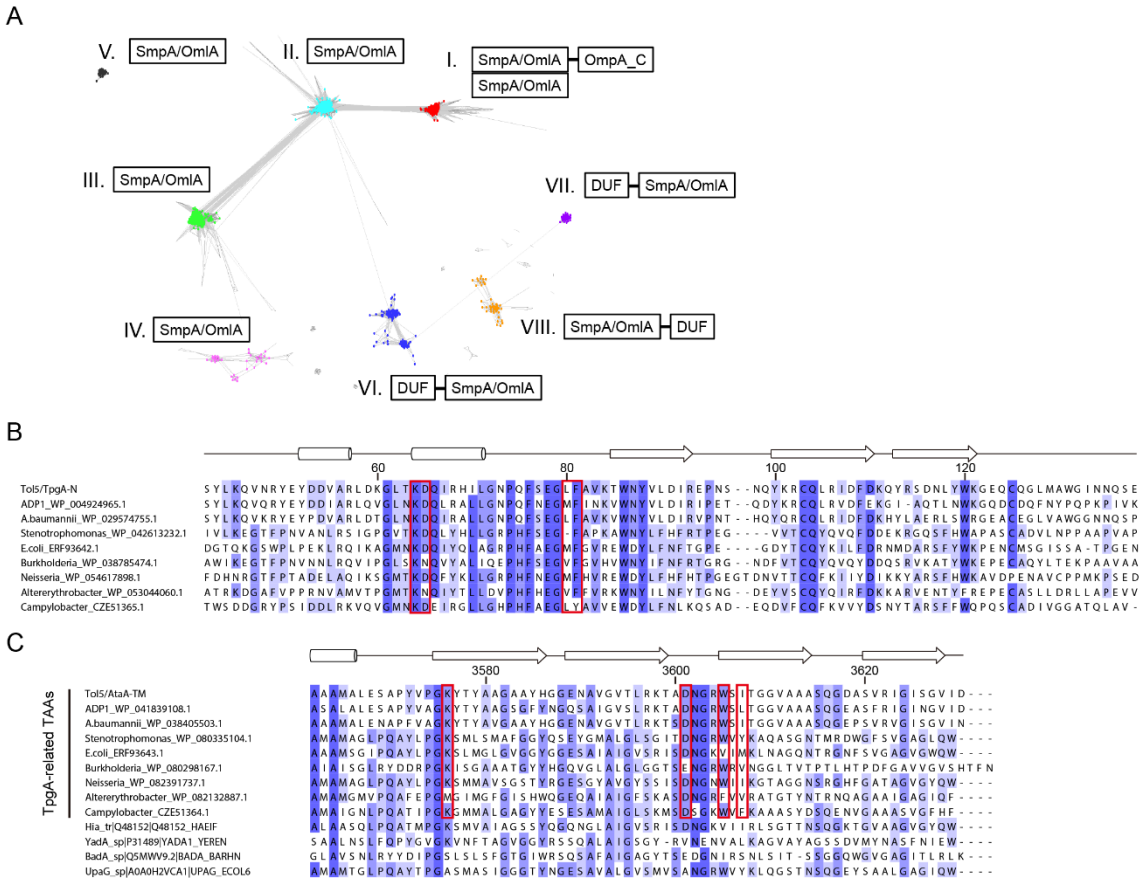

Figure 4. Bioinformatic analysis of the N-terminal domain of TpgA and the transmembrane domain of AtaA. (A) Cluster map of SmpA/OmlA family proteins. The map represents individual proteins and their sequence similarities as dots and gray lines, respectively. Note that the TpgA of Tol 5 is located in cluster I. (B) Amino acid sequence of the TpgA-N and TpgA-like proteins found in cluster I. Red boxes indicate residues that interact with AtaA. (C) Amino acid sequence of the C-terminal domain of AtaA; other TAAs found upstream of *tpgA*-like genes in the genome; and four representative TAAs (Hia, YadA, BadA, and UpaG) not related to TpgA. The red boxes indicate residues that interact with TpgA.

580

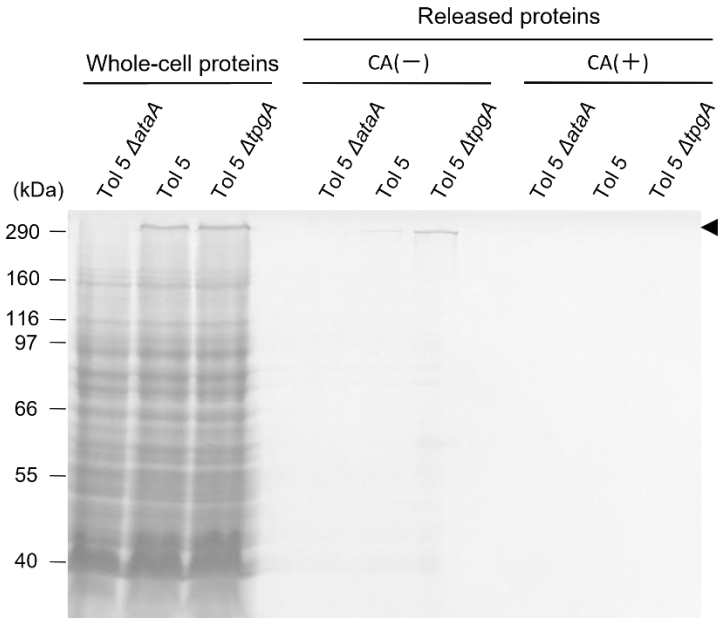

581

582 **Figure 5. Proteins released into the supernatant.** Whole-cell proteins and proteins
583 released into the supernatant after 36 h of incubation with Tol 5 or Tol 5 derivative cells
584 mixed by inversion were separated by SDS–PAGE followed by CBB staining. The black
585 arrowhead indicates bands corresponding to AtaA. CA: casamino acids, an adhesion
586 inhibitor of AtaA.

587

588

589

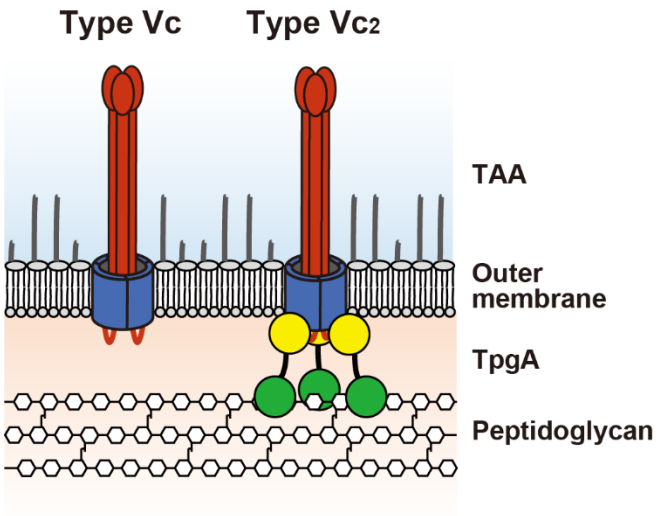

590

591 **Figure 6. Schematic representation of the type Vc2 SS.** The passenger and
592 transmembrane domains of TAAs are shown in red and blue, respectively. The N-terminal
593 and C-terminal domains of TpgA are shown in yellow and green, respectively.
594